The Search for Protoplanets with Aperture Masking (SPAM) Survey: Progress Update and Close-in Small Grain Protoplanetary Disk Features

Christina Vides[a], Steph Sallum[a], Josh Eisner[b], Andy Skemer[c], and Ruth Murray-Clay[c]

[a]Department of Physics and Astronomy, University Of California, Irvine, 4129 Frederick Reines Hall, Irvine, CA, United States
[b]Department of Astronomy and Steward Observatory, University of Arizona, Tucson, AZ, Uniteed States
[c]Astronomy & Astrophysics Department, University of California, Santa Cruz, CA, United States

ABSTRACT

Protoplanetary disks are the best places for observing planetary embryos. Direct imaging coupled with interferometric techniques, such as non-redundant masking (NRM), can help us better understand gas giant accretion timescales and dynamical interactions by resolving protoplanetary disks that exhibit evidence of planet formation. By using NRM we can achieve angular resolution down to and within the diffraction limit, and image planet formation on solar system scales (down to $\sim$ 3-7 AU for K and L band, respectively) given the distances to most young stars ($\sim$150 pc). We present progress on a NRM imaging survey designed to search for protoplanets embedded in protoplanetary disks. The goals of this survey are to detect and characterize protoplanets at solar system scales in a significant sample of protoplanetary disks and to characterize disk structure and dynamical interactions. From this survey, we can place constraints on the underlying protoplanet population and timescales under which giant gas planets form at spatial separations down to $\sim$3-7 AU.

Keywords: Near-Infrared, Circumstellar Disks, Protoplanets, Aperture Masking Interferomtery

1. INTRODUCTION

Transition disks have long been identified as active sites of planet formation. They have historically been characterized by their spectral energy distributions (SEDs), which exhibit deficits in the near-IR (NIR) followed by excesses in the mid-IR, which indicate inner regions lacking warm dust and farther out dusty regions decreasing in temperature.[1] These substructures have been confirmed in millimeter and scattered light images that display rings and gaps that may be caused by planets carving out material within the disk, and spirals and warping that may be caused by dynamic planet-disk interactions.[2–4] Other indications of ongoing planet formation within transition disks are their stellar accretion rate deficits, or lack of stellar accretion compared to full protoplanetary disks.[5] This may be due to the interception of infalling material by rapidly accreting protoplanets.[5]

High-angular resolution imaging surveys of transition disks can access the spatial separations necessary to directly characterize the physics of planet formation, such as planetary accretion timescales. Such studies can also constrain the dust distributions of the inner regions of these disks, which would allow us to understand the locations of active planet formation, as well as migration processes, which are known to play a critical role in planet formation.[6,7] Theoretical predictions of protoplanet SEDs suggest that they have low contrasts ($10^{-2} - 10^{-3}$) at NIR wavelengths (3-5μm).[8] Consequently, a high-angular resolution survey at NIR wavelengths allows for characterization of scattered light by dust reservoirs in the disk, while simultaneously searching for protoplanets.

Further author information: (Send correspondence to C.V)
C.V.: E-mail: videsc@uci.edu

Optical and Infrared Interferometry and Imaging IX, edited by Jens Kammerer, Stephanie Sallum, Joel Sanchez-Bermudez, Proc. of SPIE Vol. 13095, 1309511
 · 0277-786X · doi: 10.1117/12.3019330

To date, only two confirmed direct detections of actively forming planets have been made, PDS 70 b and c, with orbits of 21 AU and 35 AU.[9] These two protoplanets, which have extreme masses and orbits compared to the majority of mature planets, suggest a hidden population of actively forming planets that have yet to be discovered. The lack of detection of this population may be due in part to the distances of transition disks. Nearby star-forming regions are located $\gtrsim$ 100 pc away, where the angular resolutions provided by traditional direct imaging methods are insufficient for IR planet searches on orbital scales of $\lesssim 10-15$ AU.[10]

Resolving smaller scales at such distances requires interferometric techniques. One method is non-redundant masking (NRM), where a conventional telescope is turned into an interferometric array by placing a mask with discrete holes in the pupil plane.[11] NRM allows for moderate contrast (∼1:100-1:1000) at smaller angular separations ($\gtrsim 0.5\lambda$/D) than those probed by traditional imaging techniques such as coronagraphy.[12–15] From NRM observables, we can both fit models and reconstruct images to identify companion candidates and/or extended disk features. This method has been successful in probing close-in protoplanetary disk structures[16–18] and identifying companions.[19]

Here we present a progress update on the Search for Protoplanets with Aperture Masking (SPAM) survey, the highest angular resolution NIR direct imaging transition disk survey. This is achieved by using NRM and Keck/NIRC2 to image 30 known transition disks at L′, with follow-up observations executed at multiple wavelengths (i.e. K′, L′, and Ms bands). The goals of the SPAM survey are to (1) search for, detect, and characterize rapidly accreting giant protoplanets at solar-system scales in a significant sample of protoplanetary disks, (2) characterize disk structure and dynamical planet-disk interactions, and (3) place statistical constraints on the underlying protoplanet population and timescales under which they form. The SPAM survey will allow us to constrain the underlying protoplanet population to within ∼ 15% for orbits larger than 7 AU, at 95% confidence. We describe our methodology in Section 2 and our results in Section 3. We summarize the paper in Section 4.

2. METHODS

2.1 NRM

When NRM is applied, the image on the detector, or the interferogram, shows the interference fringes formed by the mask.[11] We take the Fourier transform of the interferogram to get the complex visibilities, which give the amplitudes and phases associated with the mask baselines. The complex visibility for each baseline is located in an extended region in Fourier space due to the finite size of the holes and the wavelength coverage set by the observing bandpass. From the appropriate regions in Fourier space, we calculate two quantities: squared visibilities and closure phases. Squared visibilities are the squares of the complex visibility amplitudes, and give the power corresponding to each baseline.[20] Closure phases are sums of phases around baselines that form a triangle.[21] Closure phases are highly sensitive to asymmetries and cancel first order wavefront errors, leaving only intrinsic phase and higher order residual errors. We then fit models to the Fourier observables to better understand the source brightness distribution (see Section 2.3).

2.2 Observations

As part of the SPAM survey, we have observed 30 T Tauri and Herbig Ae/Be stars located in star forming regions (typical distance of ∼150 pc) with known transition disks. We use Keck2/NIRC2 with NRM and adaptive optics (AO) to image the science targets and point spread function (PSF) calibrators. Throughout each observation, we alternate between observing a science target and multiple PSF calibrators, which are used to estimate higher order wavefront errors, spending an equal amount of time on both (∼1.7 hrs per target type per half night). To choose appropriate PSF calibrators, we optimize between matching wavefront sensor brightnesses for similar quality AO correction, brightnesses at the science wavelength for efficient integration times, and separations on the sky to maximize common atmospheric paths and minimize slew times. For each observation, we take 10 images each in the top corner and bottom corner of the detector to perform background subtraction. In order to maximize Fourier coverage, we observe the science target and PSF calibrators for 0.5 nights centered on transit. After observations, the data are reduced with a well-tested pipeline (`SAMpy`[22,23]).

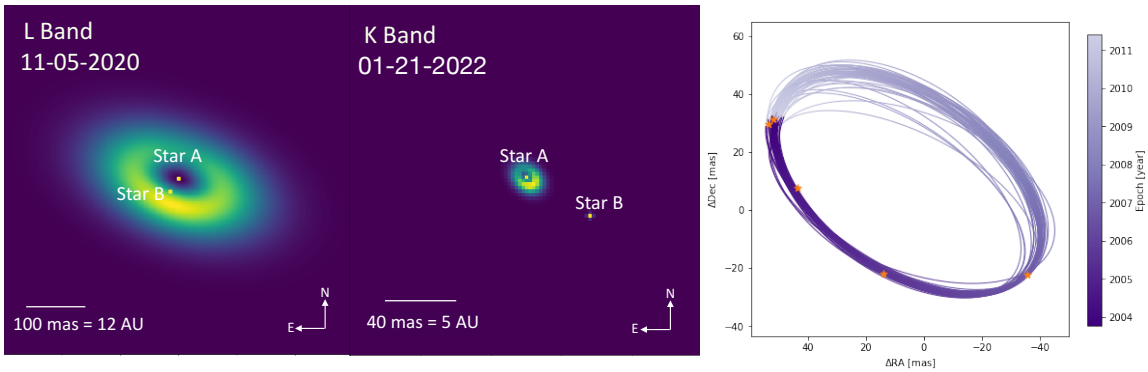

Figure 1: Left: The best-fit geometric model for L′ observations of the V892 Tau binary and circumbinary disk. The L′ observations were taken in 2020. The central star is labeled as Star A and the position of the binary companion is labeled as Star B. Middle: The best-fit geometric model to the K′ data for V892 Tau, which reveals a newly discovered circumprimary disk with a major axis of ∼2 au. The image has been cropped and zoomed-in for visualization. The K′ observations were taken in 2022, and the position angle evolution of Star B is consistent with predictions based on previous orbital estimates. Right: The orbital trajectory of Star B which includes astrometry from 24 and 25 in addition to the new NRM constraints. Here we show 50 random orbits sampled from the posterior distribution. Adapted from 18.

2.3 Image Reconstruction and Model Fitting

Closure phases and squared visibilities can be used to understand the source brightness distribution via both image reconstruction and model fitting. We reconstruct images of the targets with `SQUEEZE`,[26] an algorithm that uses Markov-Chain Monte Carlo (MCMC) methods to fit a model image to the closure phases and squared visibilities. We run SQUEEZE in parallel tempering mode to efficiently explore the image parameter space. All image reconstructions shown in this paper have a platescale of 5 milliarcseconds (mas) per pixel and a size of 100 pixels on each side. Since image reconstruction alone cannot completely recover phase information, geometric models are also required to understand the detailed morphology of the image. In addition to image reconstruction, for the targets presented here, we fit geometric disk models to the data as described in Vides et al. 2023 (18).

3. RESULTS

3.1 Survey Progress

As of 2024, we have observed 30 transition disks at L′ band, and followed up 3 of these disks at K′ band for higher angular resolution data. For five targets, we have detected scattered light from small grain disk material close to the star. Of these detections, four of the disk geometries have been characterized (see Section 3.2). We have 8 deep non-detections where we place upper limits on the masses of companions, which will be published in a future paper. We use these non-detections, along with contrast estimates for datasets currently under-analysis, to calculate the detectable protoplanet masses times accretion rates (see Section 3.3). Of the remaining targets, 16 are under-analysis and in one we identified a companion candidate which shows evidence of orbital motion over long time baselines (∼2 yr). However, future follow-up observations are required for its confirmation.

3.2 Small-Scale Disk Detections

3.2.1 V892 Tau

The V892 Tau binary system was imaged at both L′ and K′ in 2020 and 2022, respectively. As described in Vides et al. 2023,[18] we fit geometric models to the data representing circumstellar disks and stellar companions. At L′, we detect a cirumbinary disk with a ∼26 AU major axis, as expected from previous studies.[24,25] The stellar

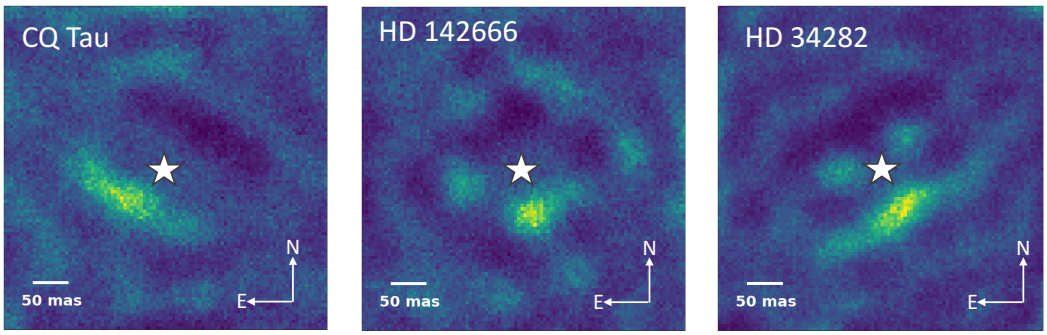

Figure 2: The SQUEEZE image reconstructions for CQ Tau (left), HD 142666 (middle) and HD 34282 (right). We find extended emission with azimuthal asymmetries in all three images that may indicate dynamical planet-disk interactions.

companion is located ∼4 AU from the primary at ∼147° measured east-of-north (Figure 1 left). At K′, we detect a circumprimary disk component with a major axis of ∼2 AU. The stellar companion is located ∼6 AU with a position angle evolution of ∼90° between the two data sets (Figure 1 middle). Using this astrometry, we update the orbit of the stellar companion (Figure 1 right) and place orbital constraints on the stellar companion.[18] We identify tentative warping in the circumbinary disk consistent with previous imaging and update the small-scale architecture to include a circumprimary component.

3.2.2 CQ Tau

Figure 2 (left) shows the reconstructed image from L′ observations of CQ Tau. Given the distance to CQ Tau (∼150 pc), we probe separations down to ∼6 AU. We detect extended emission with an azimuthal asymmetry southeast of the star in the reconstructed image that has a separation of 0.″1 (∼ 15 AU). This feature seems to be a continuity of a spiral arm located northeast of the star in lower resolution L′ images (0.″2-0.″4).[27,28] This detection of a close-in spiral arm demonstrates the high angular resolution capabilities of NRM. The spiral arm could be driven by an undetected ∼7 M_J planet outside of the L′ spiral at ∼60 AU.[28] Higher angular resolution and/or higher sensitivity imaging with future ELTs or JWST, respectively, could resolve tighter orbital separations (ELTs) or place higher contrast constraints on the wide-separation planet (JWST).

3.2.3 HD 142666

Figure 2 (middle) shows the reconstructed image of HD 142666. We detect an azimuthal asymmetry in the SQUEEZE image reconstruction located directly south of the star. We fit geometric models with the same methodology as V892 Tau, and find a highly inclined disk (∼58°) with a 0.″1 major axis (∼7 AU given a distance of ∼148 pc[29]). This measurement is consistent with the inclination and on-sky major axis position angle from model fitting to previously-published H- and K-band data.[30] However, since the previous NIR studies fit forward scattering models of simple disk rims, the disk asymmetry is forced to 90° from the major axis. We allow our disk asymmetry to be a free parameter in the geometric models. The inconsistency in the asymmetry location between the H- and K- band model images and the L′ band geometric models may indicate a warp or spiral resolved by NRM. We are currently testing other disk models to further characterize the disk geometry.

3.2.4 HD 34282

Figure 2 (right) shows the SQUEEZE image reconstructions of the HD 34282 disk. We find point-like sources east and northwest, about 50 mas from the central star each. The image also shows a larger, extended feature 50 mas southwest of the central star. These features are generally consistent with reconstructions of inclined disk rims.[31,32] This morphology is also consistent with polarimetric VLT/SPHERE/IRDIS images of HD 34282, which showed that the structure of the disk is possibly double-ringed.[33] However, the detection of the inner

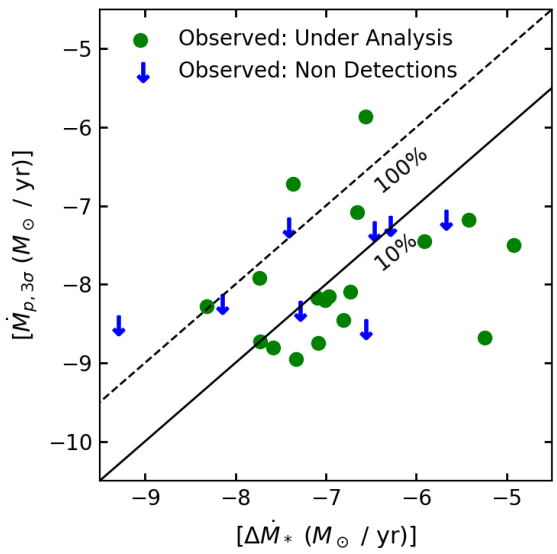

Figure 3: Detectable accretion rates (in $M_\odot$/yr) onto 1 M_J planets versus stellar accretion rate deficits (in units of $M_\odot$/ yr and defined as the difference between the stellar accretion rate and the expected accretion rate for a full disk based on the relation derived in Najita et al. 2015[5]). Blue arrows represent upper limits derived from non-detections, calculated from contrast limits (described in Section 3.3 of Vides et al. 2023[18]). Green dots represent estimates based on achievable NIRC2/NRM contrast limits for all under analysis targets. The dashed line represents the accretion rate that is 100% the stellar accretion rate deficit, while the solid line is 10%. For the majority of the targets in this survey, we are sensitive to 1 M_J planets with accretion rates that are 10% of the stellar accretion rate deficit.

disk was considered tentative since the southwest side was within the inner working angle of the SPHERE coronagraph. Our image has a similar morphology to the VLT/SPHERE/IRDIS image, and we are currently performing modeling to test the double-ringed disk scenario.

3.3 Planet Mass Times Accretion Rate Sensitivity

Transition disks have lower stellar accretion rates as a function of disk mass than full disks, occupying a separate region of this parameter space. This may be due to the interception of circumstellar material falling onto the star by rapidly accreting protoplanets.[5] Here we explore SPAM's detectable planet masses times accretion rates, in particular in the context of transition disk stellar accretion rate deficits. We define these accretion rate deficits as the differences between the known stellar accretion rates and the expected accretion rates for full protplanetary disks based on the relation derived in Najita et al. 2015.[5]

We calculate the NIRC2/NRM achievable contrasts for all targets, as described in Section 3.3 of Vides et al. 2023.[18] For each target, we convert contrast to accretion luminosity using the brightness of the central star. From the accretion luminosity, we calculate the detectable accretion rate onto a 1 M_J planet that has a circumplanetary disk with an inner radius of 2 R_J and an outer radius of 0.3 times the Hill radius.[8] Figure 3 shows the 3-σ detectable accretion rates onto 1 M_J planets versus stellar accretion rate deficits. For the majority of the targets in this survey, we are sensitive to planets accreting at 10% the stellar accretion rate deficit, demonstrating high sensitivity to accretion interception.

4. SUMMARY

We present a progress update on the SPAM survey, including tentative small-grain disk detections (CQ Tau and HD 34282) and more detailed disk geometry characterization (V892 Tau and HD 142666). The disks discussed in this paper all display azimuthal asymmetries indicative of planet-disk interactions.[2–4] Detailed geometric modeling and confirmation of the architectures of CQ Tau, HD 142666, and HD 34282 will be the subject of upcoming papers. Furthermore, follow-up observations of these objects with next generation ELT observatories and JWST will improve on these constraints and may increase planet detections.

We also calculate planet mass times accretion rate sensitivity for all non-detections and under analysis targets in the survey. From the SPAM survey, we will be able to place tight estimates on planet mass times accretion rates of detected protoplanets and place upper limits for non-detections. Given the sample size and assuming binomial statistics, the expected uncertainty on the protoplanet population at 95% confidence is ∼15%, and in the event that we do not detect any protoplanets, we will be able to determine that the underlying protoplanet

fraction down to ∼7 AU is <4% at 95% confidence. A significant number of non-detections could mean that planets in these systems are currently below our detection limits, either because they accreted the majority of their mass by an age of ∼ 2 Myr or they are low mass and accreting rapidly. Alternatively, non-detections could also indicate that the locations of rapidly-accreting planets are within our resolution limits. These direct constraints will impact our understanding of planet formation physics by informing planet formation timescales and protoplanet population statistics.

REFERENCES

[1] Strom, K. M., Strom, S. E., Edwards, S., Cabrit, S., and Skrutskie, M. F., "Circumstellar material associated with solar-type pre-main-sequence stars - A possible constraint on the timescale for planet building," **97**, 1451–1470 (May 1989).

[2] Cazzoletti, P., van Dishoeck, E. F., Pinilla, P., Tazzari, M., Facchini, S., van der Marel, N., Benisty, M., Garufi, A., and Pérez, L. M., "Evidence for a massive dust-trapping vortex connected to spirals. Multi-wavelength analysis of the HD 135344B protoplanetary disk," **619**, A161 (Nov 2018).

[3] Cieza, L. A., Casassus, S., Pérez, S., Hales, A., Cárcamo, M., Ansdell, M., Avenhaus, H., Bayo, A., Bertrang, G. H. M., Cánovas, H., Christiaens, V., Dent, W., Ferrero, G., Gamen, R., Olofsson, J., Orcajo, S., Osses, A., Peña-Ramirez, K., Principe, D., Ruíz-Rodríguez, D., Schreiber, M. R., van der Plas, G., Williams, J. P., and Zurlo, A., "ALMA Observations of Elias 2-24: A Protoplanetary Disk with Multiple Gaps in the Ophiuchus Molecular Cloud," **851**, L23 (Dec 2017).

[4] Dong, R., Liu, S.-y., Eisner, J., Andrews, S., Fung, J., Zhu, Z., Chiang, E., Hashimoto, J., Liu, H. B., Casassus, S., Esposito, T., Hasegawa, Y., Muto, T., Pavlyuchenkov, Y., Wilner, D., Akiyama, E., Tamura, M., and Wisniewski, J., "The Eccentric Cavity, Triple Rings, Two-armed Spirals, and Double Clumps of the MWC 758 Disk," **860**, 124 (Jun 2018).

[5] Najita, J. R., Andrews, S. M., and Muzerolle, J., "Demographics of transition discs in Ophiuchus and Taurus," **450**, 3559–3567 (July 2015).

[6] Monnier, J. D., Tuthill, P. G., Ireland, M., Cohen, R., Tannirkulam, A., and Perrin, M. D., "Mid-Infrared Size Survey of Young Stellar Objects: Description of Keck Segment-Tilting Experiment and Basic Results," **700**, 491–505 (July 2009).

[7] Dawson, R. I. and Murray-Clay, R. A., "Giant Planets Orbiting Metal-rich Stars Show Signatures of Planet-Planet Interactions," **767**, L24 (Apr 2013).

[8] Eisner, J. A., "Spectral Energy Distributions of Accreting Protoplanets," **803**, L4–L8 (Apr. 2015).

[9] Haffert, S. Y., Bohn, A. J., de Boer, J., Snellen, I. A. G., Brinchmann, J., Girard, J. H., Keller, C. U., and Bacon, R., "Two accreting protoplanets around the young star PDS 70," *Nature Astronomy* **3**, 749–754 (Jun 2019).

[10] Guyon, O., Eisner, J. A., Angel, R., Woolf, N. J., Bendek, E. A., Milster, T. D., Ammons, S. M., Shao, M., Shaklan, S., Levine, M., Nemati, B., Martinache, F., Pitman, J., Woodruff, R. A., and Belikov, R., "Simultaneous Exoplanet Characterization and Deep Wide-field Imaging with a Diffractive Pupil Telescope," **767**, 11 (Apr. 2013).

[11] Tuthill, P. G., Monnier, J. D., Danchi, W. C., Wishnow, E. H., and Haniff, C. A., "Michelson Interferometry with the Keck I Telescope," **112**, 555–565 (Apr. 2000).

[12] Mawet, D., Pueyo, L., Lawson, P., Mugnier, L., Traub, W., Boccaletti, A., Trauger, J. T., Gladysz, S., Serabyn, E., Milli, J., Belikov, R., Kasper, M., Baudoz, P., Macintosh, B., Marois, C., Oppenheimer, B., Barrett, H., Beuzit, J.-L., Devaney, N., Girard, J., Guyon, O., Krist, J., Mennesson, B., Mouillet, D., Murakami, N., Poyneer, L., Savransky, D., Vérinaud, C., and Wallace, J. K., "Review of small-angle coronagraphic techniques in the wake of ground-based second-generation adaptive optics systems," in [*Space Telescopes and Instrumentation 2012: Optical, Infrared, and Millimeter Wave*], **8442**, 844204 (Sept. 2012).

[13] Guyon, O., Pluzhnik, E. A., Kuchner, M. J., Collins, B., and Ridgway, S. T., "Theoretical Limits on Extrasolar Terrestrial Planet Detection with Coronagraphs," **167**, 81–99 (Nov. 2006).

[14] Ruane, G., Mawet, D., Riggs, A. J. E., and Serabyn, E., "Scalar vortex coronagraph mask design and predicted performance," in [*Society of Photo-Optical Instrumentation Engineers (SPIE) Conference Series*], *Society of Photo-Optical Instrumentation Engineers (SPIE) Conference Series* **11117**, 111171F (Sept. 2019).

[15] Sallum, S. and Skemer, A., "Comparing nonredundant masking and filled-aperture kernel phase for exoplanet detection and characterization," *Journal of Astronomical Telescopes, Instruments, and Systems* **5**, 018001 (Jan 2019).

[16] Sallum, S., Skemer, A. J., Eisner, J. A., van der Marel, N., Sheehan, P. D., Close, L. M., Ireland, M. J., Males, J. M., Morzinski, K. M., Bailey, V. P., Briguglio, R., and Puglisi, A., "New Spatially Resolved Imaging of the SR 21 Transition Disk and Constraints on the Small-grain Disk Geometry," **883**, 100 (Sept. 2019).

[17] Sallum, S., Eisner, J., Skemer, A., and Murray-Clay, R., "Systematic Multiepoch Monitoring of LkCa 15: Dynamic Dust Structures on Solar System Scales," **953**, 55 (Aug. 2023).

[18] Vides, C. L., Sallum, S., Eisner, J., Skemer, A., and Murray-Clay, R., "High-angular-resolution Imaging of the V892 Tau Binary System: A New Circumprimary Disk Detection and Updated Orbital Constraints," **958**, 123 (Dec. 2023).

[19] Ireland, M. J. and Kraus, A. L., "The Disk Around CoKu Tauri/4: Circumbinary, Not Transitional," **678**, L59–L62 (May 2008).

[20] Jennison, R. C., "A phase sensitive interferometer technique for the measurement of the Fourier transforms of spatial brightness distributions of small angular extent," **118**, 276 (1958).

[21] Baldwin, J. E., Haniff, C. A., Mackay, C. D., and Warner, P. J., "Closure phase in high-resolution optical imaging," **320**, 595–597 (Apr. 1986).

[22] Sallum, S. and Eisner, J., "Data Reduction and Image Reconstruction Techniques for Non-redundant Masking," *The Astrophysical Journal Supplement Series* **233**, 9 (Nov. 2017).

[23] Sallum, S., Ray, S., and Hinkley, S., "SAMpy: a Fourier-plane pipeline for JWST/NIRISS aperture masking interferometry (and more!)," in [*Optical and Infrared Interferometry and Imaging VIII*], Mérand, A., Sallum, S., and Sanchez-Bermudez, J., eds., *Society of Photo-Optical Instrumentation Engineers (SPIE) Conference Series* **12183**, 121832M (Aug. 2022).

[24] Monnier, J. D., Tannirkulam, A., Tuthill, P. G., Ireland , M., Cohen, R., Danchi, W. C., and Baron, F., "Discovery of a Circumbinary Disk around Herbig Ae/Be System V892 Tauri," **681**, L97 (Jul 2008).

[25] Long, F., Andrews, S. M., Vega, J., Wilner, D. J., Chandler, C. J., Ragusa, E., Teague, R., Pérez, L. M., Calvet, N., Carpenter, J. M., Henning, T., Kwon, W., Linz, H., and Ricci, L., "The Architecture of the V892 Tau System: The Binary and Its Circumbinary Disk," **915**, 131 (July 2021).

[26] Baron, F., Monnier, J. D., and Kloppenborg, B., "A novel image reconstruction software for optical/infrared interferometry," in [*Optical and Infrared Interferometry II*], **7734**, 77342I (July 2010).

[27] Hammond, I., Christiaens, V., Price, D. J., Ubeira-Gabellini, M. G., Baird, J., Calcino, J., Benisty, M., Lodato, G., Testi, L., Pinte, C., Toci, C., and Fedele, D., "External or internal companion exciting the spiral arms in CQ Tau?," **515**, 6109–6121 (Oct. 2022).

[28] Uyama, T., Muto, T., Mawet, D., Christiaens, V., Hashimoto, J., Kudo, T., Kuzuhara, M., Ruane, G., Beichman, C., Absil, O., Akiyama, E., Bae, J., Bottom, M., Choquet, E., Currie, T., Dong, R., Follette, K. B., Fukagawa, M., Guidi, G., Huby, E., Kwon, J., Mayama, S., Meshkat, T., Reggiani, M., Ricci, L., Serabyn, E., Tamura, M., Testi, L., Wallack, N., Williams, J., and Zhu, Z., "Near-infrared Imaging of a Spiral in the CQ Tau Disk," **159**, 118 (Mar. 2020).

[29] Gaia Collaboration, "VizieR Online Data Catalog: Gaia EDR3 (Gaia Collaboration, 2020)," *VizieR Online Data Catalog* , I/350 (Nov. 2020).

[30] Davies, C. L., Kraus, S., Harries, T. J., Kreplin, A., Monnier, J. D., Labdon, A., Kloppenborg, B., Acreman, D. M., Baron, F., Millan-Gabet, R., Sturmann, J., Sturmann, L., and Ten Brummelaar, T. A., "Simultaneous Spectral Energy Distribution and Near-infrared Interferometry Modeling of HD 142666," **866**, 23 (Oct 2018).

[31] Sallum, S., Eisner, J., Close, L. M., Hinz, P. M., Follette, K. B., Kratter, K., Skemer, A. J., Bailey, V. P., Briguglio, R., Defrere, D., Macintosh, B. A., Males, J. R., Morzinski, K. M., Puglisi, A. T., Rodigas, T. J., Spalding, E., Tuthill, P. G., Vaz, A., Weinberger, A., and Xomperio, M., "Imaging protoplanets: observing transition disks with non-redundant masking," in [*Optical and Infrared Interferometry and Imaging V*], **9907**, 99070D (Aug. 2016).

[32] Cheetham, A., Huélamo, N., Lacour, S., de Gregorio-Monsalvo, I., and Tuthill, P., "Near-IR imaging of T Cha: evidence for scattered-light disc structures at Solar system scales," **450**, L1–L5 (June 2015).

[33] de Boer, J., Ginski, C., Chauvin, G., Ménard, F., Benisty, M., Dominik, C., Maaskant, K., Girard, J. H., van der Plas, G., Garufi, A., Perrot, C., Stolker, T., Avenhaus, H., Bohn, A., Delboulbé, A., Jaquet, M., Buey, T., Möller-Nilsson, O., Pragt, J., and Fusco, T., "Possible single-armed spiral in the protoplanetary disk around HD 34282," **649**, A25 (May 2021).